

# Rate-Dependent Role of $I_{Kur}$ in Human Atrial Repolarization and Atrial Fibrillation Maintenance

Martin Aguilar,<sup>1,2</sup> Jianlin Feng,<sup>3</sup> Edward Vigmond,<sup>4,5</sup> Philippe Comtois,<sup>1,2</sup> and Stanley Nattel<sup>1,6,7,8,9,\*</sup>

<sup>1</sup>Research Center, Montreal Heart Institute and <sup>2</sup>Department of Pharmacology and Physiology/Institute of Biomedical Engineering, Université de Montréal, Montreal, Québec, Canada; <sup>3</sup>Bristol-Myers Squibb, Wallingford, Connecticut; <sup>4</sup>L'Institut de Rythmologie et Modélisation Cardiaque LIRYC, Fondation Université de Bordeaux, Hôpital Xavier-Arnoz, Pessac, France; <sup>5</sup>Institut de Mathématiques de Bordeaux, Université de Bordeaux, Talence, France; <sup>6</sup>Department of Medicine and <sup>7</sup>Department of Pharmacology and Therapeutics, McGill University, Montreal, Québec, Canada; <sup>8</sup>Department of Medicine, Université de Montréal, Montreal, Québec, Canada; and <sup>9</sup>West German Heart and Vascular Center, Faculty of Medicine, University Duisburg-Essen, Essen, Germany

**ABSTRACT** The atrial-specific ultrarapid delayed rectifier  $K^+$  current ( $I_{Kur}$ ) inactivates slowly but completely at depolarized voltages. The consequences for  $I_{Kur}$  rate-dependence have not been analyzed in detail and currently available mathematical action-potential (AP) models do not take into account experimentally observed  $I_{Kur}$  inactivation dynamics. Here, we developed an updated formulation of  $I_{Kur}$  inactivation that accurately reproduces time-, voltage-, and frequency-dependent inactivation. We then modified the human atrial cardiomyocyte Courtemanche AP model to incorporate realistic  $I_{Kur}$  inactivation properties. Despite markedly different inactivation dynamics, there was no difference in AP parameters across a wide range of stimulation frequencies between the original and updated models. Using the updated model, we showed that, under physiological stimulation conditions,  $I_{Kur}$  does not inactivate significantly even at high atrial rates because the transmembrane potential spends little time at voltages associated with inactivation. Thus, channel dynamics are determined principally by activation kinetics.  $I_{Kur}$  magnitude decreases at higher rates because of AP changes that reduce  $I_{Kur}$  activation. Nevertheless, the relative contribution of  $I_{Kur}$  to AP repolarization increases at higher frequencies because of reduced activation of the rapid delayed-rectifier current  $I_{Kr}$ . Consequently,  $I_{Kur}$  block produces dose-dependent termination of simulated atrial fibrillation (AF) in the absence of AF-induced electrical remodeling. The inclusion of AF-related ionic remodeling stabilizes simulated AF and greatly reduces the predicted antiarrhythmic efficacy of  $I_{Kur}$  block. Our results explain a range of experimental observations, including recently reported positive rate-dependent  $I_{Kur}$ -blocking effects on human atrial APs, and provide insights relevant to the potential value of  $I_{Kur}$  as an antiarrhythmic target for the treatment of AF.

## INTRODUCTION

The ultrarapid delayed rectifier  $K^+$  current ( $I_{Kur}$ ) was originally described as a rapidly activating, 4-aminopyridine-sensitive  $K^+$  current with slow and limited inactivation (1). However, many of the original experiments used relatively short test pulses, typically <4 s long, which may have not been enough to observe the full extent of  $I_{Kur}$ 's inactivation. Feng et al. (2), using longer 50-s test pulses, showed that  $I_{Kur}$  inactivates almost completely when the cell is depolarized to +40 mV, with a biexponential time course comprising fast ( $\tau_f$ ) and slow time constants ( $\tau_s$ ) of 1.0 and 6.8 s, respectively. Based on these experiments, it

has been hypothesized that  $I_{Kur}$  inactivation may play an important role under physiological conditions, specifically related to  $I_{Kur}$  frequency-dependent dynamics (2). The potential for full inactivation of  $I_{Kur}$  suggests that the contribution of the current would decrease at faster rates, as the total amount of time when the cell is depolarized increases and inactivation accumulates. However, recent experimental results using the  $I_{Kur}$ -selective blocker XEN-D0103 suggest the opposite, and indicate that the contribution of  $I_{Kur}$  to atrial repolarization increases at higher rates (3).

To our knowledge, none of the commonly used mathematical models of the human atrial cardiomyocyte action potential (AP) integrate the experimentally defined  $I_{Kur}$  inactivation dynamics reported by Feng et al. (2). To better understand the rate-dependent role of  $I_{Kur}$  and the effect of blocking it on the human atrial AP, it is necessary to use a model with accurate inactivation properties. In this study, we sought to 1) quantify the kinetic features of the  $I_{Kur}$

Submitted November 21, 2016, and accepted for publication March 23, 2017.

\*Correspondence: stanley.nattel@icm-mhi.org

Philippe Comtois and Stanley Nattel contributed equally to this work.

Editor: Eric Sobie.

<http://dx.doi.org/10.1016/j.bpj.2017.03.022>

© 2017 Biophysical Society.



inactivation properties defined by Feng et al. (2); 2) update the Courtemanche human atrial AP model (4) to include realistic  $I_{Kur}$  inactivation parameters; 3) investigate the rate-dependent properties of  $I_{Kur}$  inactivation over the course of the AP under physiological conditions; 4) evaluate the contribution of  $I_{Kur}$  with realistic inactivation properties to human atrial repolarization at different frequencies; and 5) evaluate the potential consequences for effects of blocking  $I_{Kur}$  on atrial fibrillation (AF) in non-remodeled and AF-remodeled atrial tissue.

## MATERIALS AND METHODS

### Mathematical modeling of $I_{Kur}$ inactivation

The experimental data recorded by Feng et al. (2) were used as the basis for model development in our study. A description of the experimental methods can be found in the original article (2). The Courtemanche human atrial cardiomyocyte model was implemented (4). The original formulation of the  $I_{Kur}$  inactivation parameter is as follows:

$$I_{Kur} = C_m \times g_{Kur} \times u_a^3 \times u_i \times (V - E_K),$$

$$g_{Kur} = 0.005 + \frac{0.05}{1 + \exp\left(-\frac{V - 15}{13}\right)},$$

$$\alpha_{ui} = \left[21 + \exp\left(-\frac{V - 185}{28}\right)\right]^{-1},$$

$$\beta_{ui} = \exp\left(\frac{V - 158}{16}\right),$$

$$\tau_{ui} = [\alpha_{ui} + \beta_{ui}]^{-1} / K_{Q10},$$

$$u_{i,\infty} = \left[1 + \exp\left(\frac{V - 99.45}{27.48}\right)\right]^{-1},$$

$$\frac{du_i}{dt} = \frac{u_{i,\infty} - u_i}{\tau_{ui}},$$

where  $I_{Kur}$  is the ultrarapid delayed rectifier  $K^+$  current,  $g_{Kur}$  is the maximal  $I_{Kur}$  conductance,  $V$  is the transmembrane potential,  $E_K$  is the  $K^+$  equilibrium potential, and  $u_a$  and  $u_i$  are  $I_{Kur}$ 's activation and inactivation gating variables, respectively;  $\alpha_{ui}$  and  $\beta_{ui}$  are the forward and backward rate constants for the inactivation gate variable, respectively;  $\tau_{ui}$  is the time constant;  $u_{i,\infty}$  is the steady-state relation for the inactivation gate variable;  $C_m$  is the membrane capacitance (100 pF); and  $K_{Q10}$  is a scaling factor (3). To account for  $I_{Kur}$  inactivation dynamics we replaced the original inactivation gating variable  $u_i$  by fast ( $u_{i,f}$ ) and slow ( $u_{i,s}$ ) inactivation gating variables. The gating variables and time constant parameters were fitted by iteratively minimizing the mean error of the model time constants relative to experimentally derived values obtained with a 50-s test-pulse at 0, 10, 20, 30, 40, and 50 mV (Fig. S1, B and C); the modified inactivation gating variables and time constants are given by the following:

$$\tau_{uif} = 800 \times \left(2 - \left[\frac{V}{40}\right]\right),$$

$$u_{i,f\infty} = \left[1 + \exp\left(\frac{V - 35}{20}\right)\right]^{-1},$$

$$\tau_{uis} = 5800 \times \left[1 + \exp\left(-\frac{V + 80}{11}\right)\right]^{-1},$$

$$u_{i,s\infty} = \left[1 + \exp\left(\frac{V + 5}{5}\right)\right]^{-1},$$

$$\frac{du_{i,x}}{dt} = \frac{u_{i,x\infty} - u_{i,x}}{\tau_{uix}},$$

$$I_{Kur} = C_m \times g_{Kur} \times u_a^3 \times u_{i,s} \times u_{i,f} \times (V - E_K).$$

The activation gating variable and time constant were not modified and are given by the following:

$$\tau_{ua} = [\alpha_{ua} + \beta_{ua}]^{-1} / K_{Q10},$$

$$\alpha_{ua} = 0.65 \left[ \exp\left(-\frac{V + 10}{8.5}\right) + \exp\left(-\frac{V - 30}{59}\right) \right]^{-1},$$

$$\beta_{ua} = 0.65 \left[ 2.5 + \exp\left(\frac{V + 82}{17}\right) \right]^{-1},$$

$$\tau_{ua} = [\alpha_{ua} + \beta_{ua}]^{-1} / K_{Q10},$$

$$u_{a,\infty} = \left[1 + \exp\left(-\frac{V + 30.3}{9.6}\right)\right]^{-1}.$$

The activation gate open probability is given by  $u_a^3$ . The inactivation gate open probability in the original model was given by  $u_i$ ; in the modified model  $u_{i,s} \times u_{i,f}$  was used to reflect the combined effects of slow and fast inactivation components. Open probabilities range from 0 (closed) to 1 (open). The charge carried by  $I_{Kur}$  in one cardiac cycle, given by the area under the  $I_{Kur}$ -versus-time curve (Kur AUC), was calculated by integrating  $I_{Kur}$  over one cardiac cycle. The activation gate open-probability area under the curve ( $u_a^3$  AUC) was calculated by integrating  $u_a^3$  over one cardiac cycle. The AP amplitude was defined as the difference between the peak phase-0 overshoot potential and the resting membrane potential.

### Mathematical simulations

The Courtemanche model of human atrial cardiomyocyte bioelectricity was implemented with the original and updated  $I_{Kur}$  inactivation formulations. The total ionic current for the model ( $I_{tot}$ ) was given by the following:

$$I_{tot} = I_{Na} + I_{K1} + I_{to} + I_{Kur} + I_{Kr} + I_{Ks} + I_{Ca,L} + I_{p,Ca} \\ + I_{NaK} + I_{NaCa} + I_{b,Na} + I_{b,Ca} + I_{K,ACh},$$

where  $I_{Na}$  is the fast inward  $Na^+$  current;  $I_{K1}$  is the inward rectifier  $K^+$  current;  $I_{to}$  is the transient outward  $K^+$  current;  $I_{Kur}$ ,  $I_{Kr}$ , and  $I_{Ks}$  are the ultra-rapid, rapid, and slow components of the delayed rectifier  $K^+$  current, respectively;  $I_{Ca,L}$  is the L-type inward  $Ca^{2+}$  current;  $I_{p,Ca}$  is the sarcolemmal  $Ca^{2+}$  pump current;  $I_{NaK}$  is the  $Na^+/K^+$  pump current;  $I_{NaCa}$  is the  $Na^+/Ca^{2+}$  exchanger current;  $I_{b,Na}$  is the background  $Na^+$  current;  $I_{b,Ca}$  is the background  $Ca^{2+}$  current; and  $I_{K,ACH}$  is the acetylcholine-activated  $K^+$  current (5). Isolated cardiomyocyte APs were simulated at 37°C by numerical integration with the software MATLAB's ODE23s ordinary differential equation solver (The MathWorks, Natick, MA) with a relative tolerance of  $10^{-2}$ . For each condition, pacing was sustained for 280 cycles with 2-ms 3 nA stimuli and the last action potential was used for analysis.

Computer simulations of the effect of  $I_{Kur}$  block on AF were performed with the CARP simulator, which solves the monodomain equation by the finite element method as described previously (6), as follows:

$$\nabla \times \sigma_i \nabla V = \beta \left( C_m \frac{\partial V}{\partial t} + I_{tot} \right),$$

where  $\sigma_i$  is the tissue conductivity,  $\beta$  is the membrane surface-to-volume ratio ( $0.14 \mu m^{-1}$ ), and  $C_m$  is the membrane capacitance ( $1 \mu F/cm^2$ ). The updated Courtemanche ionic model was adapted and implemented in CARP. Conductivities were chosen to give a physiological conduction velocity in the longitudinal direction (47.9 cm/s). The tissue measured  $7 \times 6$  cm with fibers oriented along the long dimension with an anisotropy ratio of  $\sim 6$ . The grid was discretized at 100- $\mu m$  resolution and equations solved with a 25- $\mu s$  timestep. Reentry was initiated by a standard S1-S2 cross-shock protocol with an S1-S2 interval of 170 ms.

Two-dimensional simulations were conducted using three different acetylcholine (ACh) distribution patterns (one homogeneous ACh distribution and two sinusoidal distributions) and three peak ACh concentrations (1.875, 3.75, and 7.5 nM), generating nine conditions.  $I_{Kur}$  block was simulated by a fixed reduction in maximal  $I_{Kur}$  conductance ( $g_{Kur}$ ). Dose-response curves were generated by introducing  $I_{Kur}$  block at 10 different time-points ( $t_{drug} = 1000$  ms, 1100 ms, ... 1800 ms, 1900 ms) for each percent  $I_{Kur}$  block {10%, 20%, ..., 90%, 100%}; the average time to termination was quantified as the time from  $t_{drug}$  to reentry termination. Simulations were run using the control (non-remodeled) Courtemanche human atrial AP model and repeated with an AF-remodeled AP model consisting of the control model with the following modifications:  $I_{to}$  conductance reduced by 50%,  $I_{Kur}$  conductance reduced by 50%,  $I_{Ca,L}$  conductance reduced by 70%, and  $I_{K1}$  conductance increased by 100% (7).

## RESULTS

### Experimentally observed time-dependent inactivation of $I_{Kur}$

The ultrarapid delayed rectifier  $K^+$  current ( $I_{Kur}$ ) is often described as having slow and partial inactivation. Fig. 1 A shows normalized  $I_{Kur}$  during a 1000 ms test-pulse to +40 mV, 5 ms after a 100-ms pretest pulse to +40 mV to inactivate  $I_{to}$ , as recorded experimentally (black) (2) and from the original Courtemanche human atrial  $I_{Kur}$  formulation (blue). Using this relatively short test pulse, experimental  $I_{Kur}$  inactivates by  $\sim 45\%$  (black). In contrast to experimental data, in the original Courtemanche model,  $I_{Kur}$  does not inactivate appreciably over the course of the pulse (blue). Fig. 1 B shows normalized  $I_{Kur}$  during a longer, 50 s test-pulse to +40 mV, 5 ms after a 100-ms pretest pulse to +40 mV to inactivate  $I_{to}$ . With the longer pulse, the experimentally recorded  $I_{Kur}$  (black) inactivated

completely with a biexponential time-course characterized by fast and slow time constants of  $702 \pm 7$  and  $5688 \pm 26$  ms, respectively. Again, the original Courtemanche model (blue) fails to reproduce  $I_{Kur}$ 's inactivation dynamics, with 85% of the peak current persisting at the end of the 50-s test-pulse.

### Model inactivation kinetics modified according to experimental data

To accurately reproduce the experimentally recorded  $I_{Kur}$  inactivation kinetics, we modified the Courtemanche model by introducing a set of slow ( $u_{i,s}$ ) and fast ( $u_{i,f}$ ) inactivation gating variables in place of the single inactivation gating variable ( $u_i$ ) in the original model. The voltage dependence of the inactivation gating variables for the original ( $u_{i,original}$ , blue line) and modified ( $u_{i,f}$ , red solid line;  $u_{i,s}$ , red dashed line) models is shown in Fig. S1 A. The major modification to inactivation gating is more complete inactivation at depolarized potentials; the complete mathematical formulation can be found in Materials and Methods. We also replaced the inactivation time constant ( $\tau_{u_i,original}$ ) with a set of fast ( $\tau_{u_{i,f}}$ ) and slow ( $\tau_{u_{i,s}}$ ) inactivation time constants (Fig. S1 B). Note that the updated inactivation time constants are of the order of 1–6 s. The voltage dependence of the activation gating variable (Fig. S1 C;  $u_{a,x}$ ) and activation time constant (Fig. S1 D,  $\tau_{u_{a,x}}$ ) were not modified. The activation time constant is in the range of 1–6 ms.

The modified model (red line) closely reproduced the experimentally recorded current inactivation (black line) during a prolonged pulse (Fig. 1 B) and the experimentally recorded  $I_{Kur}$  inactivation kinetics (Fig. 1 C) at 37°C. Excellent agreement between experiments and the mathematical model was obtained across the spectrum of test potentials.

### Time-, voltage-, and frequency dependence of $I_{Kur}$ inactivation

We then compared the time dependence of  $I_{Kur}$  inactivation in the model to experimental results obtained by varying the duration of the test pulse. Fig. 1 D (black) shows experimentally recorded normalized  $I_{Kur}$  obtained with conditioning pulses to +40 mV of varying durations, followed by a 100-ms prepulse to +40 mV to inactivate  $I_{to}$  and then a 100-ms test pulse to +40 mV.  $I_{Kur}$  displayed complete inactivation with conditioning pulses  $>20$  s. In contrast, the original Courtemanche model-derived results showed little inactivation even with the longest conditioning-pulse duration (Fig. 1 D, blue). Conversely, the modified model closely replicated the experimental data (Fig. 1 D, red); the half-inactivation conditioning pulse duration ( $CPD_{1/2}$ ) was 1100 ms at +40 mV. The voltage dependence of  $I_{Kur}$  inactivation was then assessed by applying a 50 s pretest pulse to various voltages followed by a 240-ms test pulse to +50 mV; the experimentally

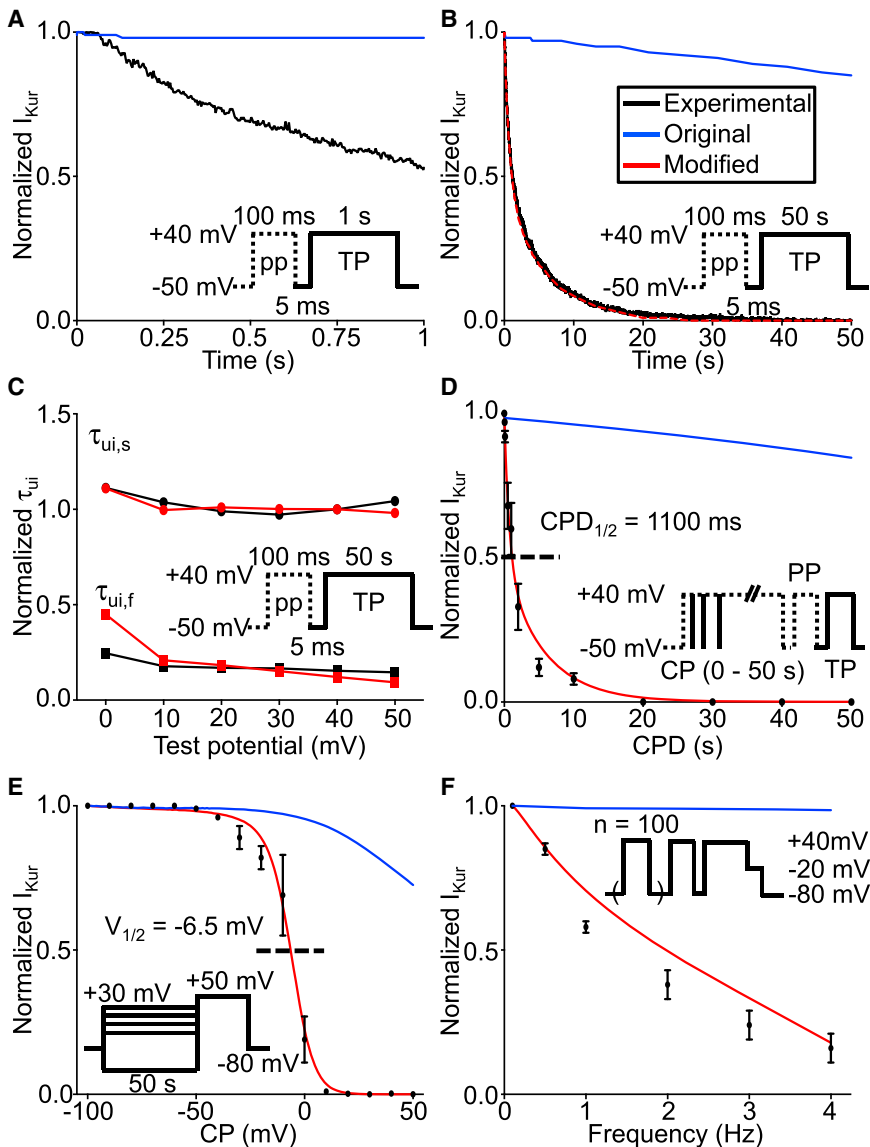


**FIGURE 1** Time-, voltage-, and frequency dependence of  $I_{K_{ur}}$  inactivation. (A) Shown here is the normalized  $I_{K_{ur}}$  current during a 1000-ms test pulse (TP) at +40 mV, 5 ms after a 100-ms prepulse (PP), to inactivate  $I_{to}$  (inset) as recorded from the experimental preparation (black) and the original Courtemanche human atrial model (blue). (B) Normalized  $I_{K_{ur}}$  current using a similar protocol, but with test pulse duration of 50 s as recorded from the experimental preparation (black) and the original and modified Courtemanche model (blue and red, respectively), is given. The experimental and modified model time constants are  $\tau_{ui,f,exp} = 702 \pm 7$  ms,  $\tau_{ui,s,exp} = 5688 \pm 26$  ms and  $\tau_{ui,f,model} = 713 \pm 18$  ms,  $\tau_{ui,s,model} = 5848 \pm 188$  ms, respectively. (C) Normalized fast ( $\tau_{ui,f}$ ) and slow ( $\tau_{ui,s}$ ) time constants as a function of test pulse potential for the experimental preparation and the modified Courtemanche model at 37°C are shown. (D) Shown here is the normalized  $I_{K_{ur}}$  current using a CPD to +40 mV, followed by a 100-ms prepulse (PP) to +40 mV to inactivate  $I_{to}$  preceding a 100-ms test pulse (TP) to +40 mV (inset), as recorded from the experimental preparation and the original and modified models; the half-inactivation CPD ( $CPD_{1/2}$ ) was 1100 ms. (E) Shown here is the normalized  $I_{K_{ur}}$  current using a 50 s-conditioning pulse (CP) to various voltages followed by a 240-ms test pulse to +50 mV (inset); the half-inactivation voltage ( $V_{1/2}$ ) was -6.5 mV in the model and  $-7.5 \pm 0.6$  mV experimentally. (F) Shown here is the normalized  $I_{K_{ur}}$  current obtained by applying 100 pretest stimuli of 100 ms duration at +40 mV at various frequencies, followed by a 100-ms conditioning pulse to +40 mV to inactivate  $I_{to}$  and a 140-ms test pulse to +40 mV (inset); the normalized current at 4 Hz was 16% of its value at 0.1 Hz. For all panels, experimental data are in black; original and modified models are in blue and red, respectively.

recorded normalized  $I_{K_{ur}}$  is shown in Fig. 1 E (black).  $I_{K_{ur}}$  inactivation is highly dependent on the pretest pulse potential. The original Courtemanche model (blue) did not reproduce the experimentally observed voltage-dependent inactivation dependence (Fig. 1 E, black), whereas the modified model-generated results (red) closely matched experimental findings. The experimental and modified-model half-inactivation voltages ( $V_{1/2}$ s) were  $-7.5 \pm 0.6$  and  $-6.5$  mV, respectively.

The frequency dependence of  $I_{K_{ur}}$  inactivation was studied by applying 100 pulses of 100-ms duration to +40 mV at various frequencies, followed by a 100-ms conditioning pulse to +40 mV to inactivate  $I_{to}$  and a 140-ms test pulse to +40 mV. Experimentally,  $I_{K_{ur}}$  displayed marked frequency dependence with 84% reduction at 4 vs. 0.1 Hz (Fig. 1 F, black data). In contrast, the original Courtemanche model showed virtually no frequency dependence

(Fig. 1 F, blue). The modified model was much more consistent with the experimental findings (Fig. 1 F, red).

### Incorporation of realistic $I_{K_{ur}}$ inactivation kinetics and AP dynamics

Fig. S2 shows the AP amplitude (Fig. S2 A), AP duration at 90% repolarization ( $APD_{90}$ , Fig. S2 B), transmembrane potential at the time of maximum phase 0 overshoot (overshoot potential, Fig. S2 C), and phase-0 peak  $Na^+$  current (peak  $I_{Na}$ , Fig. S2 D) as a function of cycle length (CL) for the original (black) and modified (red) Courtemanche models. Despite markedly different  $I_{K_{ur}}$  inactivation kinetics, there were no significant differences in AP or  $Na^+$ -current dynamics between the two models across a wide range of physiologically relevant cycle lengths. We then pursued the rate-dependent properties of  $I_{K_{ur}}$  to understand why,



despite much greater inactivation for both experimental and model pulse protocols than in the original Courtemanche model, there was no apparent effect on rate-dependent AP properties.

### $I_{Kur}$ activation and inactivation dynamics and mechanisms of rate-dependence

Fig. 2 A shows model APs at progressively shorter stimulation cycle lengths (750, 500, 300, and 265 ms). The AP duration is shortened and plateau potential becomes less positive as the dome disappears when stimulation cycle length decreases. Fig. 2 B shows the corresponding  $I_{Kur}$  simulations. There is a rate-dependent decrease in  $I_{Kur}$  during phase 2 of the AP with little change in peak  $I_{Kur}$  (inset) except at the shortest cycle length (inset, red). Fig. 2, C and D, shows the corresponding activation and inactivation gate open probabilities ( $u_a^3$ ;  $u_{i,f} \times u_{i,s}$ ) as a function of time for the shortest (red) and longest (blue) cycle length.  $I_{Kur}$  activation decreases during phase 2 in a rate-dependent manner (Fig. 2 C), whereas inactivation is virtually rate independent (Fig. 2 D). Therefore,  $I_{Kur}$  rate dependence is driven by its activation gate kinetics, with little contribution from inactivation. This is further detailed in Fig. S3 where the rate dependence of the total  $I_{Kur}$  charge carried per cycle (Fig. S3 B) is shown to be due to changes in rate-dependent activation-gate open probability (Fig. S3 F), with no significant contribution from inactivation (Fig. S3 D).

Fig. 2 E shows the steady-state activation gating variable as a function of transmembrane potential with the voltage for 50% ( $V_{0.5} = -30$  mV) activation marked with a purple

dot;  $V_{0.5}$  is shown in Fig. 2 A as a purple dashed line. For membrane potentials negative to  $V_{0.5}$ , the activation gate starts to close, whereas for potentials positive to  $V_{0.5}$ , the activation gate is mostly open. The activation-variable ( $u_a^3$ ; Fig. 2 C) rate dependence can be understood based on the AP time course (Fig. 2 A) and  $u_a$ 's voltage dependence (Fig. 2 E). At slower stimulation frequencies like a cycle length of 750 ms (blue curve in Fig. 2 A), the plateau potential is positive to  $V_{0.5}$  (dashed purple line in Fig. 2 A) for the duration of phase 2 of the AP, keeping  $u_a$  largely open. It is only at the end of the AP plateau that the membrane potential falls below  $V_{0.5}$ , leading to appreciable decreases in  $u_a$  and return of the activation gate open probability toward 0 ( $u_a^3 = 0$ , closed, Fig. 2 C). In contrast, at faster stimulation frequencies such as at a cycle length of 265 ms (red curve in Fig. 2 A), the plateau potential is negative to  $V_{0.5}$  starting at the end of phase 1 (Fig. 2 A), leading to earlier and more rapid closure of the activation gate (red curve in Fig. 2 C). The activation-gate time constant is in the range of 1–6 ms (Fig. S1 D), which allows the activation gate to closely track changes in membrane potential.

Fig. 2 F shows the fast ( $u_{i,f}$ , solid black line) and slow ( $u_{i,s}$ , black dashed line) inactivation gating variables as a function of test potential, with the slow inactivation-gating variable  $V_{0.5}$  marked by a teal dot. For membrane potentials positive to  $V_{0.5}$  (teal dot), the slow inactivation gate starts to close whereas for membrane potentials negative to  $V_{0.5}$ , the inactivation gates are mostly open. Fig. 2 D shows the inactivation gate open probability ( $u_{i,f} \times u_{i,s}$ ) as a function of time at stimulation cycle lengths of 265 ms (red) and 750 ms (blue). The rate independence of  $u_{i,f} \times u_{i,s}$  (Fig. 2 D,

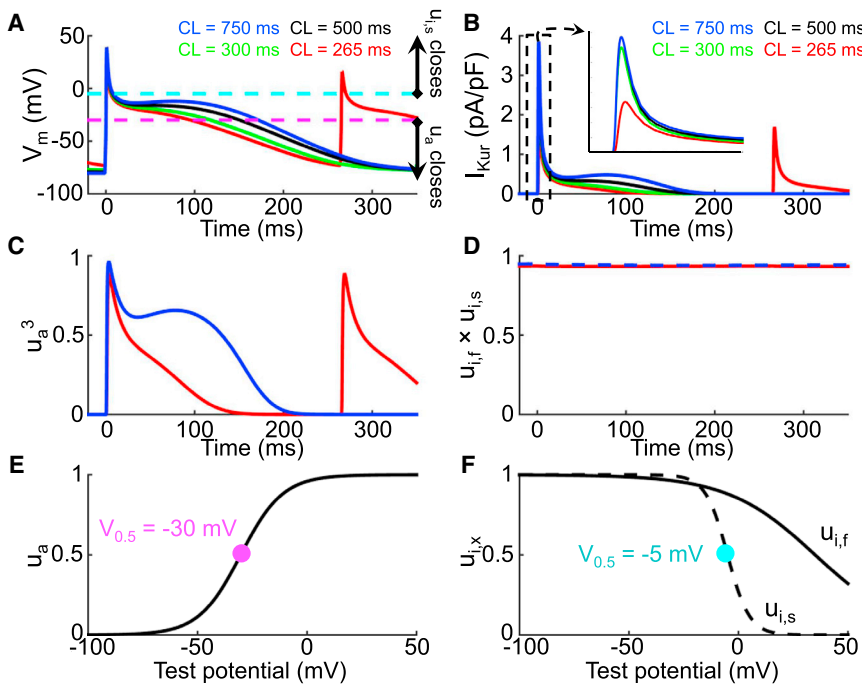


FIGURE 2 Mechanism of  $I_{Kur}$  rate dependence. (A) Action potentials at stimulation cycle lengths from 265 ms (red), 300 ms (green), 500 ms (black), and 750 ms (blue) are shown. The purple and teal dashed lines correspond to the activation and inactivation gating variable 50% ( $V_{0.5,ua} = -30$  mV and  $V_{0.5,uis} = -5$  mV) opening potentials, respectively. (B) Shown here are corresponding  $I_{Kur}$  tracings; there is a rate-dependent decrease in  $I_{Kur}$  during phase 2 of the AP. (C) Shown here is the activation gate open probability ( $u_a^3$ ) and (D) inactivation gate open probability ( $u_{i,f} \times u_{i,s}$ ) as a function of time for CLs of 265 ms (red) and 750 ms (blue). The activation open probability is rate dependent and the inactivation open probability is rate independent. (E) Shown here is the activation gating variable ( $u_a$ ) as a function of transmembrane potential; the purple dot corresponds to activation gating variable  $V_{0.5}$  as transposed on (A). (F) Fast ( $u_{i,f}$ , black solid) and slow ( $u_{i,s}$ , black dashed) inactivation gating variables as a function of transmembrane potential are given; the teal dot corresponds to the slow inactivation gating variable  $V_{0.5}$  as transposed on (A). The inactivation open probability is rate independent because the action potential spends very little time positive to  $V_{0.5,uis}$  ( $-5$  mV; teal).

blue versus red) can be explained from the AP time course (Fig. 2 A) and  $u_i$ 's voltage dependence (Fig. 2 F). For the slow inactivation gate to close, the membrane potential needs to be positive to  $V_{0.5}$  ( $-5$  mV). For the fast inactivation variable, the voltage dependence is even more positive. However, the AP, both at cycle lengths of 265 and 750 ms, spends negligible time at potentials positive to the  $V_{0.5}$  of either fast or slow inactivation (positive to the blue-dashed line in Fig. 2 E). Moreover, the inactivation time constants are  $>1$  s (Fig. S1 B), at least two orders-of-magnitude longer than the time the membrane spends above  $V_{0.5}$ . Hence, because the membrane spends very little time positive to  $V_{0.5}$  and the inactivation gate time constants are slow to close, the inactivation gating variables remain mostly in their open state ( $>0.93$  fractional availability, Fig. 2 D) irrespective of activation frequency.

### Rate-dependent effects of $I_{Kur}$ block on AP properties and underlying mechanism

When  $I_{Kur}$  is blocked, the plateau voltage is raised and  $I_{Kr}$  is enhanced, counteracting the repolarization delays caused by  $I_{Kur}$  block (8). Consequently, to understand the rate-dependent AP changes caused by  $I_{Kur}$  block, it is essential to analyze the associated changes in  $I_{Kr}$ . Fig. 3 A shows the steady-state  $I_{Kr}$  activation-gate variable in the Courtemanche model as a function of test potential, with  $V_{0.1}$  ( $-28$  mV),  $V_{0.5}$  ( $-14$  mV),  $V_{0.75}$  ( $-7$  mV), and  $V_{0.9}$  ( $0$  mV) marked and transposed as dashed lines onto Fig. 3 B. Fig. 3, B–D, shows the AP,  $I_{Kur}$ , and  $I_{Kr}$  simulations obtained at a cycle length of 1000 ms under control conditions (blue) and with 75%  $I_{Kur}$  block (red).  $I_{Kur}$  block elevates the plateau potential,

bringing the membrane potential positive to  $I_{Kr}$ 's  $V_{0.5}$  ( $-14$  mV; green dashed line in Fig. 3 B) for the duration of phase 2 of the AP, leading to a 136% increase in  $I_{Kr}$ , an acceleration in phase-3 repolarization and no net change in overall APD (Fig. 3 B;  $APD_{-60}$  control versus  $I_{Kur}$  block = 255 vs. 256 ms, respectively). Fig. 3, E–G, shows the AP,  $I_{Kur}$ , and  $I_{Kr}$  simulations at a cycle length of 250 ms under control conditions (blue) and with 75%  $I_{Kur}$  block (red). Because of the change in AP morphology at the short cycle length,  $I_{Kur}$  block-induced elevation of the plateau fails to keep the plateau potential in the  $I_{Kr}$  activation range (e.g.,  $V_{0.5}$  of  $-14$  mV; green dashed line in Fig. 3 E), hence, there is little  $I_{Kr}$  recruitment (ratio of total  $I_{Kr}$  with  $I_{Kur}$  block versus control = 1.40), leading to APD prolongation ( $APD_{-60}$  under control versus  $I_{Kur}$ -block conditions of 199 and 209 ms, respectively). Therefore, despite the fact that  $I_{Kur}$  is smaller at rapid frequencies, the ability of  $I_{Kur}$  block to prolong APD is enhanced.

### $I_{Kur}$ block and AF termination

The above analysis suggests that the APD-prolonging effect of  $I_{Kur}$  blockade is preserved at rapid rates and might result in an ability to suppress AF. We therefore studied the effect of  $I_{Kur}$  block on simulated two-dimensional cholinergic AF. We generated nine ACh conditions (Fig. S4); reentry was sustained for  $>5$  s across conditions but displayed markedly different dynamics ranging from single spiral wave reentry (Fig. S5) to multiple, short-lived wavelets (Figs. 4, S5, and S6 for representative examples). In line with our single-cell results, there were no significant differences in reentry dynamics,  $APD_{-60}$  distribution, and depolarized

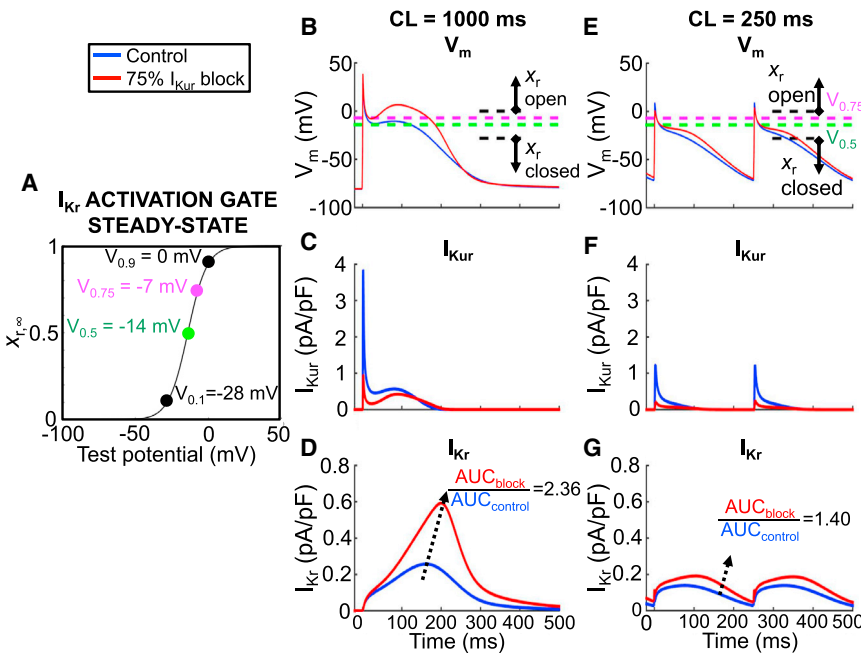


FIGURE 3 Rate-dependent effects of  $I_{Kur}$  block on the AP. (A) Shown here is the  $I_{Kr}$  activation gate steady state ( $x_{r,\infty}$ ) as a function of test potential.  $V_{0.1}$ ,  $V_{0.5}$ ,  $V_{0.75}$ , and  $V_{0.9}$  are marked and transposed onto (B) and (E) as dashed lines. (B) Shown here are APs obtained at a cycle length of 1000 ms under control (blue) and with 75%  $I_{Kur}$  blockade (red); the AP duration at  $-60$  mV ( $APD_{-60}$ ) was 255 ms for both. (C and D) Shown here are corresponding  $I_{Kur}$  and  $I_{Kr}$  tracings; the ratio of  $I_{Kr}$  with 75%  $I_{Kur}$  block to control was 2.36. (E) Shown here are APs obtained at a cycle length of 250 ms under control (blue) and with 75%  $I_{Kur}$  blockade (red); the  $APD_{-60}$  for control and 75%  $I_{Kur}$  block was 199 and 209 ms, respectively. (F and G) Shown here are corresponding  $I_{Kur}$  and  $I_{Kr}$  tracings; the ratio of  $I_{Kr}$  with 75%  $I_{Kur}$  block to control was 1.40.

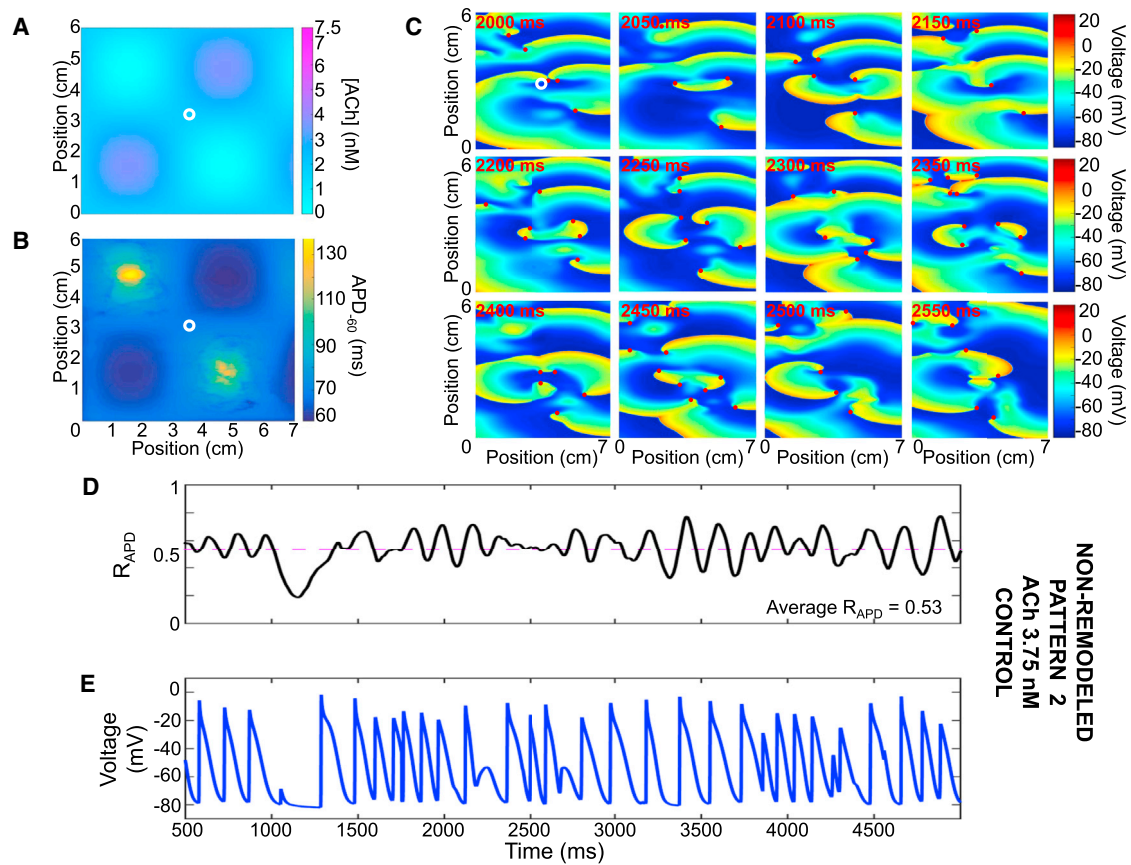


FIGURE 4 Representative example of simulated vagotonic AF using pattern #2 with a peak ACh concentration of 3.75 nM and the non-remodeled cardiomyocyte model. (A) Shown here is ACh distribution with peak concentration of 3.75 nM and (B) a corresponding APD<sub>60</sub> distribution. (C) Shown here is transmembrane potential over time at 50-ms intervals; reentry is maintained by multiple short-lived spiral waves. (D) Shown here is the ratio of depolarized cells (ratio of cells with a voltage positive to  $-60$  mV to the total number of cells) and (E) transmembrane potential over time for the cardiomyocyte marked with a white circle in (A) and (B).

fraction between the original and modified I<sub>Kur</sub> inactivation models (Figs. 5, S7, and S8 for representative examples). Using the non-remodeled Courtemanche human action potential model, we found a dose-dependent relationship between AF termination efficacy and percent I<sub>Kur</sub> block (Fig. 6). Reentry termination was relatively infrequent with  $<50\%$  I<sub>Kur</sub> block, but increased to  $>90\%$  of simulations at 100% I<sub>Kur</sub> block for all conditions considered. We also found an inverse relationship between average time to termination and percent I<sub>Kur</sub> block (Fig. 6).

Fig. 7 shows a representative example of successful AF termination by 50% I<sub>Kur</sub> block with ACh pattern #2 and a peak concentration of 3.75 nM (Fig. 7 A). The areas of largest ACh concentration had the shortest APs (Fig. 7 B). I<sub>Kur</sub> block prolonged refractoriness, increasing the excursion of the phase singularities, favoring wave-front collision, annihilation, and reentry termination (Fig. 7, C–E). Fig. S9 shows the dynamics with the same ACh pattern/concentration but with 100% I<sub>Kur</sub> block; the increased refractoriness is even more pronounced and termination more rapid. Consistent with a significant role of I<sub>Kur</sub> in AP repolarization, the mean APD<sub>60</sub> increased from 85 ms under control

conditions to 97 and 126 ms at 50 and 100% I<sub>Kur</sub> block, respectively.

We then sought to investigate whether I<sub>Kur</sub> block could successfully terminate two-dimensional AF under ionically remodeled conditions, such as in chronic AF. As previously reported (7), AF-remodeling conditions stabilize reentry dynamics (Figs. S10–S12) and ACh is no longer needed to maintain AF. Overall, the efficacy of I<sub>Kur</sub> block in terminating AF in remodeled atria was very low, with no termination observed below 80% block and 10% termination at 90 and 100% block in the absence of ACh and across the nine ACh conditions (see Fig. S13 for a representative example). At the cellular level, remodeling stabilized reentry 1) by significantly shortening the APD<sub>90</sub> (APD<sub>90</sub> for non-remodeled versus remodeled was 283 vs. 195 ms, respectively at CL 1000 ms and 204 vs. 140 ms, respectively at CL 250 ms) and 2) by hyperpolarizing the resting membrane potential (RMP) as compared to the non-remodeled cardiomyocyte (Fig. 8, A and B, dashed versus solid) across a wide range of diastolic intervals. The I<sub>Kur</sub> block-induced APD<sub>90</sub> prolongation was preserved under remodeled conditions (Fig. 8 C versus Fig. 8 D, red versus blue;  $\Delta$ APD<sub>90</sub> at



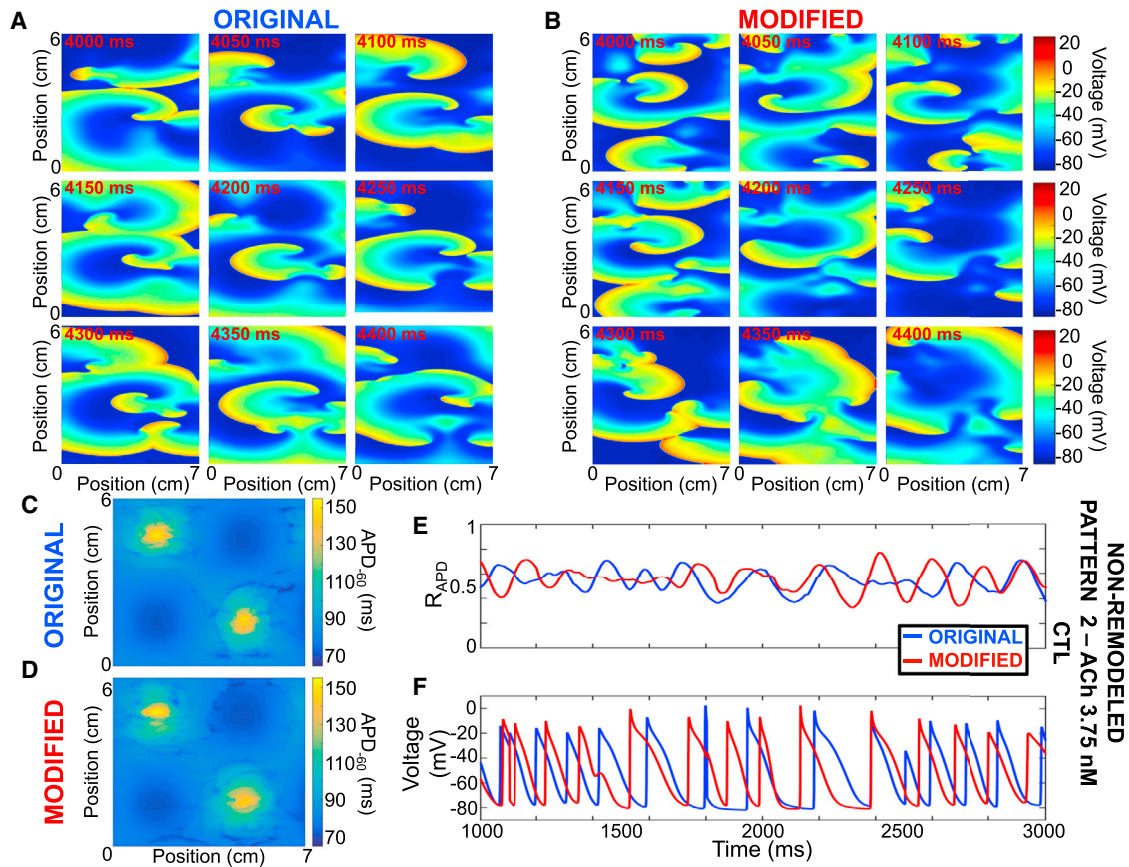


FIGURE 5 Representative example comparing reentry dynamics in the original and modified models. (A and B) Transmembrane potential snapshots over time at 50-ms intervals for the original and modified models are shown. (C and D) APD<sub>60</sub> values for the original and modified models are given. (E and F) Shown here is the ratio of depolarized cells (ratio of cells with a voltage positive to  $-60$  mV to the total number of cells) and transmembrane potential for the original (blue) and modified (red) models. Non-remodeled cardiomyocyte model with ACh pattern #2 with peak concentration of 3.75 nM is given.

CL = 250 ms non-remodeled versus remodeled was 11 vs. 10 ms, respectively). However, because the remodeled AP is of much shorter duration and is hyperpolarized, the diastolic interval is long enough for the AP to return to the RMP before the next activation, even at rapid stimulation frequencies (Fig. 8 A, blue versus red dashed). Conversely, for the non-remodeled cardiomyocyte, even a small prolongation in APD encroaches on repolarization at short CLs (Fig. 8 A, blue versus red solid), and  $I_{Kur}$  block causes APD alternans behavior at short CLs (Fig. 8 C). Hence, the differential efficacy of  $I_{Kur}$  blockade for AF termination in remodeled versus non-remodeled atria appears to be related to the remodeling-induced APD-abbreviation and hyperpolarization more than from  $I_{Kur}$  downregulation, because the APD prolongation caused by  $I_{Kur}$  block is preserved in remodeled cardiomyocytes.

## DISCUSSION

In this study, we have developed an updated formulation of  $I_{Kur}$  inactivation kinetics that reproduces experimentally observed  $I_{Kur}$  inactivation properties. Using the model, we

have shown that, under physiological stimulation conditions,  $I_{Kur}$  dynamics are mainly determined by its activation kinetics with relatively minor contribution from channel inactivation. Hence, 1) contrary to intuition,  $I_{Kur}$  inactivation does not accumulate at rapid stimulation frequencies; and 2) despite a rate-dependent decrease in absolute  $I_{Kur}$  magnitude, the relative contribution of  $I_{Kur}$  to AP repolarization increases with increased activation frequency. We also found that  $I_{Kur}$  block terminates simulated cholinergic AF in a dose-dependent fashion in non-remodeled atrial tissue but is ineffective in the presence of simulated atrial remodeling. Because  $I_{Kur}$  is expressed in the human atrium but not ventricle (9), it is an interesting potential candidate for atrial-selective anti-AF therapy. Therefore, the demonstration that despite its potential for complete inactivation,  $I_{Kur}$  maintains a significant contribution to repolarization dynamics and arrhythmia maintenance during AF, is potentially important.

## $I_{Kur}$ inactivation

The initial reports characterizing  $I_{Kur}$  inactivation used relatively short test pulses, typically  $<5$  s long, and therefore



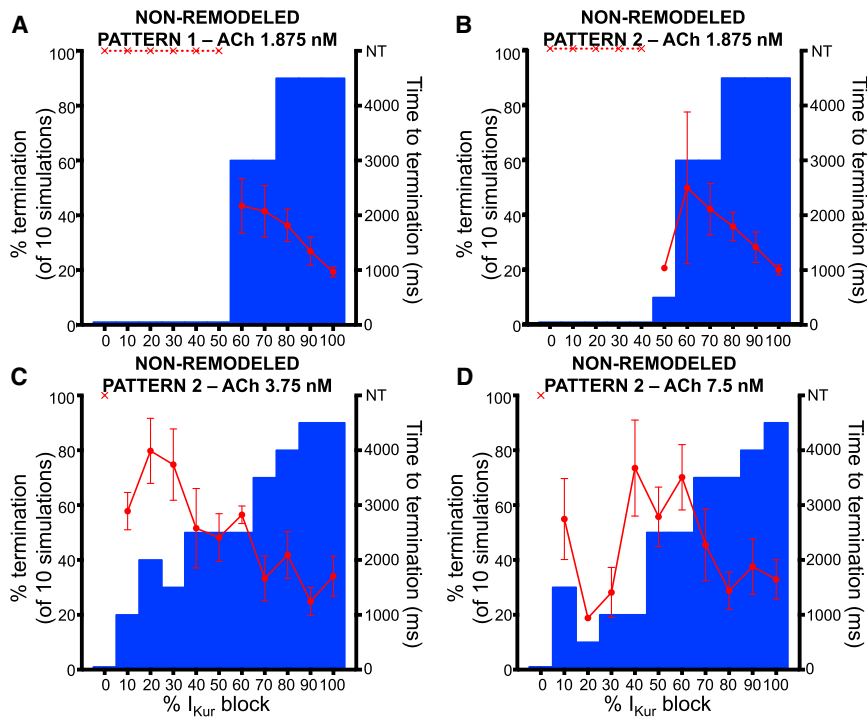


FIGURE 6 Dose-response (*bar-graphs*) and average time to termination (*red data*) by I<sub>Kur</sub> block using the non-remodeled cardiomyocyte model for (A) ACh pattern #1 with peak ACh concentration of 1.875 nM. (B–D) Shown here are the ACh pattern #2 and peak ACh concentrations of 1.875, 3.75, and 7.5 nM, respectively.

failed to observe the full scale of I<sub>Kur</sub> inactivation (1,10–14). Using 50-s test pulses, Feng et al. (2) demonstrated that human atrial I<sub>Kur</sub> inactivates fully, with a biexponential time-course characterized by rapid and slow time constants of 1.0 and 6.8 s, respectively. Moreover, I<sub>Kur</sub> inactivation was found to be highly time-, voltage-, and frequency-dependent. These observations raised the possibility that channel inactivation could accumulate at rapid activation frequencies, significantly decreasing I<sub>Kur</sub>'s contribution to AP dynamics. If I<sub>Kur</sub> inactivated completely at rapid activation frequencies, such as during AF, then I<sub>Kur</sub> blockers would be predicted to have minimal antiarrhythmic effects. Paradoxically, and contrary to this intuitive expectation, recent work with the highly selective I<sub>Kur</sub> blocker XEN-D0103 found that I<sub>Kur</sub> block prolongs the atrial APD and effective refractory period preferentially at rapid activation frequencies (3).

### Novel elements relative to prior in silico work

To our knowledge, none of the commonly used human atrial in silico models correctly reproduces the experimentally observed I<sub>Kur</sub> inactivation kinetics. In this investigation, we first analyzed experimental recordings of I<sub>Kur</sub> inactivation to produce an accurate in silico representation. We then studied I<sub>Kur</sub> inactivation dynamics and rate-dependence with the updated model that accounted realistically for I<sub>Kur</sub> inactivation (2) by introducing a set of fast and slow inactivation gating variables ( $u_{i,f}$  and  $u_{i,s}$ ) and corresponding time constants ( $\tau_{u_{i,f}}$  and  $\tau_{u_{i,s}}$ ). The modified model accurately reproduced I<sub>Kur</sub> time-, voltage-, and frequency-dependent

inactivation across a wide range of physiological test potentials. Of note, the inactivation-gate time constants are three orders-of-magnitude slower than the activation-gate time constant (second versus millisecond). After including the updated I<sub>Kur</sub> representation in the Courtemanche AP-model, we compared AP parameters as a function of stimulation cycle length and found no significant difference between the original and modified model results despite markedly different inactivation kinetics. We then applied our model to gain insight into the role of I<sub>Kur</sub> activation and inactivation on I<sub>Kur</sub> and its rate-dependent role in repolarization and arrhythmia maintenance.

### Mechanism of I<sub>Kur</sub> rate dependence

Using the modified model, we showed that the activation gate open probability is highly rate-dependent (because of rate-induced AP morphology changes) and parallels I<sub>Kur</sub> rate dependence, whereas the inactivation gate open probability is effectively rate independent because the cell spends little time at voltages associated with significant inactivation-gate closure. Hence, I<sub>Kur</sub> rate-dependence is due to its activation gating-variable dynamics and rate-dependent changes in AP morphology, with no contribution from inactivation.

### Rate-dependent effect of I<sub>Kur</sub> block on AP repolarization

We next sought to understand the mechanism underlying the positive rate-dependent effect of I<sub>Kur</sub> block on the APD, as

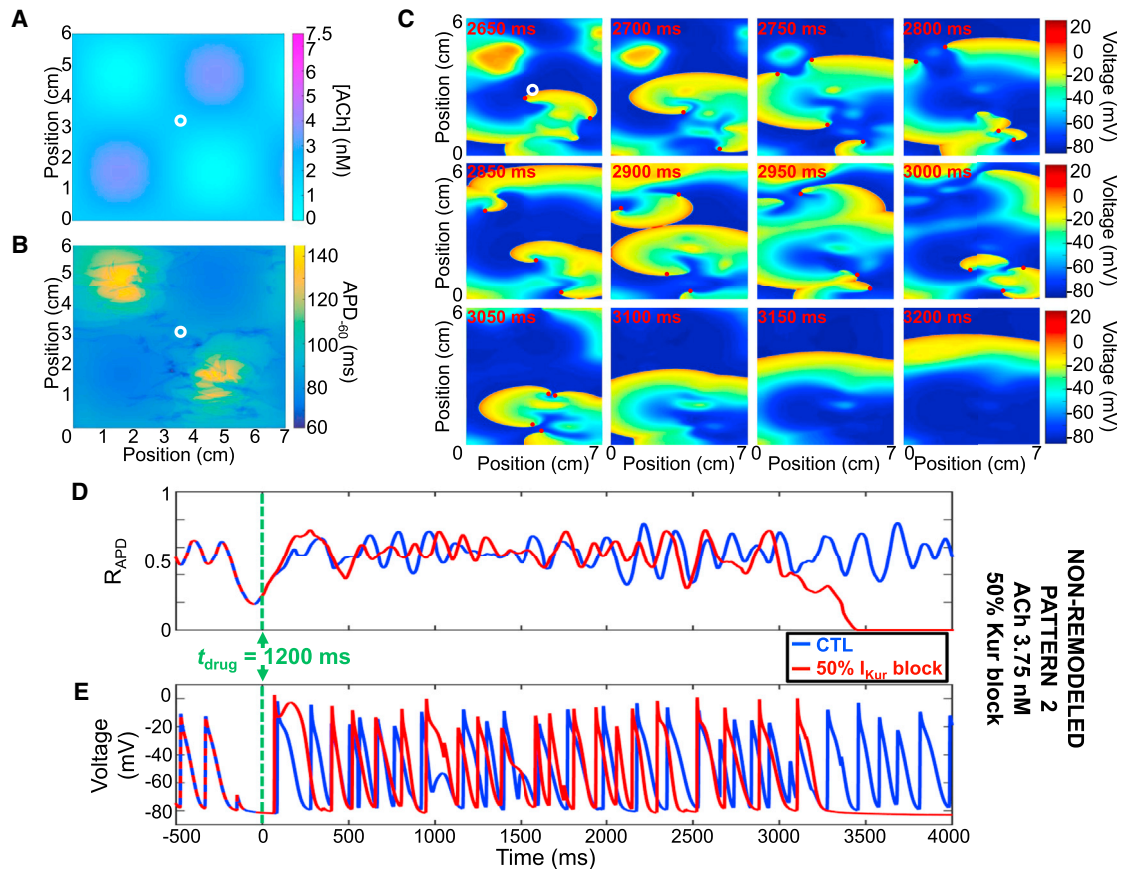


FIGURE 7 Representative example of reentry termination by 50%  $I_{Kur}$  block using ACh pattern #2 with peak ACh concentration of 3.75 nM and the non-remodeled cardiomyocyte model. (A) Shown here is the ACh distribution with peak concentration of 3.75 nM and (B) its corresponding APD<sub>-60</sub> distribution. (C) Transmembrane potential snapshots over time at 50 ms intervals are given; 50%  $I_{Kur}$  block was introduced at  $t_{drug} = 1200$  ms. (D) Shown here is the ratio of depolarized cells (ratio of cells with a voltage positive to  $-60$  mV to the total number of cells) and (E) transmembrane potential over time for the cardiomyocyte marked with a white circle in (A) and (B) for control (blue) and 50%  $I_{Kur}$  block (red).

reported by Ford et al. (3). At slow stimulation frequencies,  $I_{Kur}$  block significantly elevated the AP plateau potential compared to control (no block), keeping the membrane at potentials for which  $I_{Kr}$ 's activation gate opens for the duration of phase 2 of the AP, leading to recruitment of  $I_{Kr}$  and compensating for  $I_{Kur}$  blockade with minimal effect on the APD. At rapid stimulation frequencies, the membrane potential is negative to  $I_{Kr}$ 's half-activation potential leading to little  $I_{Kr}$  recruitment, limited compensation by  $I_{Kr}$ , and  $I_{Kur}$  block-induced APD prolongation at rapid frequencies. Hence, although  $I_{Kur}$ 's absolute magnitude is less at rapid activation frequencies, the relative contribution of  $I_{Kur}$  to AP repolarization makes  $I_{Kur}$  block a potentially interesting atrial-selective anti-AF strategy.

The mechanisms of reverse rate-dependency (RRD) of drug-induced APD changes have been a matter of substantial debate. Arguing from first principles, Zaza (15) proposed that RRD is an intrinsic property of cardiac cells and that the same change in total transmembrane current will prolong long APs more than short ones. These predictions were supported by experimental work in which APD

changes were shown to be proportional to the initial APD using clinically available drugs like the class-I agent lidocaine and class-III agent dofetilide, as well as by applying inward or outward current pulses (16). The same group suggested that channel blockers may, at best, attenuate this intrinsic RRD but that forward rate-dependency (FRD) would be "difficult to attain" (16). In an elegant study using a series of ventricular cardiomyocyte models, Cummins et al. (17) challenged this notion by suggesting that RRD can be overcome if rate-dependent AP morphological changes are large enough. In other words, the complex nonlinear rate-dependent changes in current dynamics may be such that RRD could be offset, making FRD possible. For example, they showed that increasing  $I_{Ca,L}$  ( $g_{Ca,L}$ ) leads to FRD changes by elevating the AP plateau potential, leading to differential  $I_{Ks}$  activation at slow activation frequencies (17). Because  $I_{Kur}$  is not expressed in ventricular cardiomyocytes, the possible FRD properties of  $I_{Kur}$  block could not be evaluated. Our findings in atrial cardiomyocytes are, however, qualitatively in line with these observations, because we found that  $I_{Kur}$  block moves the

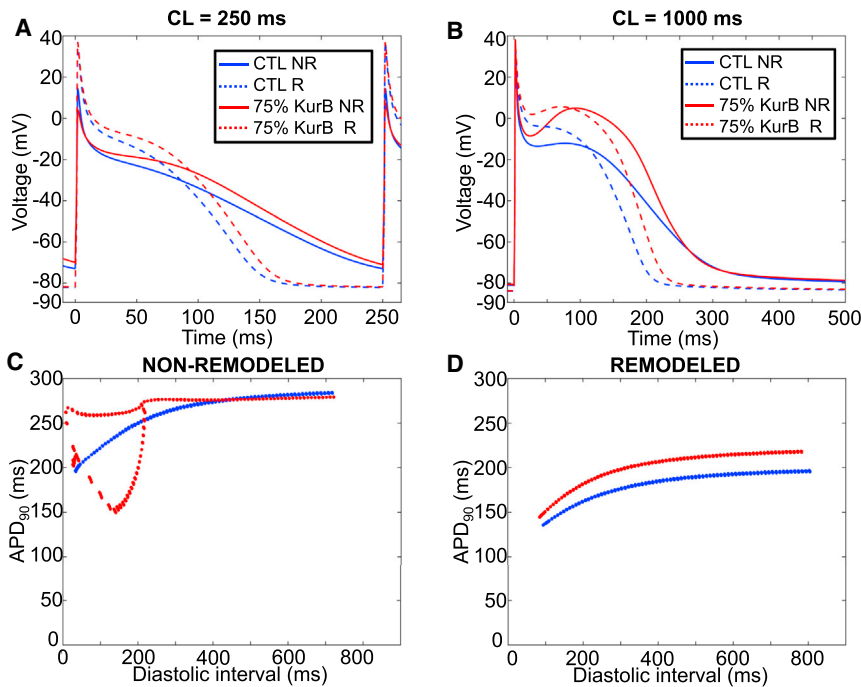


FIGURE 8  $I_{Kur}$  blocking effects in remodeled cardiomyocytes. (A) Shown here is a single cell AP at a stimulation CL of 250 ms for a non-remodeled (NR; *solid*) and remodeled (R; *dashed*) cardiomyocyte without drug (*blue*) and with 75%  $I_{Kur}$  block (*red*); (B) same as in (A), but at CL of 1000 ms. (C) Shown here is an AP at 90% repolarization ( $APD_{90}$ ) as a function of diastolic interval without drug (*blue*) and with 75%  $I_{Kur}$  block (*red*) for a non-remodeled cardiomyocyte; (D) same as in (C), but for a remodeled cardiomyocyte.

AP plateau potential to more positive voltages, leading to differential  $I_{Kr}$  activation at slow versus rapid pacing rates and FRD APD-prolongation. Hence, FRD APD-prolongation, a highly desirable antiarrhythmic property, may be an attainable goal.

### Relevance for antiarrhythmic drug development

We also found that  $I_{Kur}$  block terminates simulated cholinergic AF in a dose-dependent manner in nonionically remodeled atrial tissue by prolonging refractoriness, increasing the reentry wavelength, favoring rotor collision and annihilation. These findings are consistent with prior experimental work using relatively  $I_{Kur}$ -specific blockers in goats, rats, pigs, humans, and in silico systems (18–22). Electrical remodeling shortened the APD and hyperpolarized the RMP, leading to very stable reentry as described in Pandit et al. (7). The ability of  $I_{Kur}$  block to terminate simulated AF was greatly attenuated by remodeling, because the block-induced APD-prolongation was insufficient to counteract the strong effects of remodeling. The APD-prolonging effect of  $I_{Kur}$  block was not per se affected by channel downregulation. These observations are consistent with the report by Ford et al. (3), in which  $APD_{90}$  prolongation induced by the  $I_{Kur}$ -selective blocker XEN-D0103 was maintained in chronic-AF human atrial cardiomyocytes. Scholz et al. (22) found that  $I_{Kur}$  block was effective at terminating simulated AF, even in remodeled atria. However, they used slightly different remodeling parameters, included gap junction remodeling, and did not incorporate  $I_{Kur}$  downregulation. The differential effectiveness of  $I_{Kur}$

block in non-remodeled versus remodeled atria is consistent with a prior randomized phase-3 clinical trial in which vernakalant, a mixed  $I_{Na}/I_{Kur}$  blocker, was much less effective at restoring sinus rhythm in patients with long-lasting AF (4.0%) compared to recent-onset AF (51.7%) (23). Of note, recent experimental work demonstrated persistent antiarrhythmic efficacy of vernakalant in goats with remodeled atria owing to unaltered effects on  $Na^+$ -dependent parameters (conduction velocity and postrepolarization refractoriness) (24). Our findings suggest that the clinical efficacy of pure  $I_{Kur}$  block may be limited to recent-onset AF, in which remodeling has not taken place.

For the purposes of this study,  $I_{Kur}$  block was simulated as a fixed reduction in maximal conductance ( $g_{Kur}$ ). However, there is in silico and experimental evidence that the electrophysiological and antiarrhythmic effects of  $I_{Kur}$  blockade are modulated by the time- and voltage-dependent kinetics of block. Using a family of  $I_{Kur}$ -selective diphenyl phosphine oxide compounds, Lagrutta et al. (25) were able to show that  $I_{Kur}$  blocking potency and frequency dependence were functions of blocking kinetics, with open state blockers being the most effective  $I_{Kur}$  antagonists. Several other molecules, including vernakalant and experimental compounds like zatebradine, loratadine, and bisindolylmaleimide, have also been shown to block  $I_{Kur}$  preferentially in the open state (19,26–28). Mathematical simulations support these findings and suggest that  $I_{Kur}$  blockers with rapid binding or slow unbinding kinetics have the strongest antiarrhythmic effects (22,29). Further work is needed to analyze the effects (if any) on state-dependent drug block, of adding realistic  $I_{Kur}$  inactivation kinetics.

Consistent with this study, XEN-D0101, a selective  $I_{Kur}$  blocker, prolonged the atrial effective refractory period (AERP) and decreased AF vulnerability in a dose- and rate-dependent manner in atrial tachycardia-induced remodeled canine atria (30,31). In human cardiomyocytes, XEN-D0101 prolonged AERP in AF-remodeled but not in non-remodeled tissue (32). However, experiments were conducted using a stimulation frequency of 1 Hz at which we predict no effect on APD and AERP based on this study; rapid stimulation rates at which  $I_{Kur}$ -block induced prolongation of APD/atrial refractoriness would be expected were not reported. In coronary-perfused canine atria, 4-aminopyridine (a moderately selective  $I_{Kur}$  blocker) was found to shorten APD and to increase the propensity for AF, displaying only mildly antiarrhythmic effects in remodeled atrial tissue (33). Again, the protocol employed a stimulation cycle length of 500 ms at which  $I_{Kur}$  block would not be expected to increase the APD or AERP. Furthermore, the mechanism of  $I_{Kur}$  in dog atrium is different from that in humans, and the magnitude is often very small (34). MK-0448 failed to prolong AERP in healthy human subjects using relatively slow stimulation cycle lengths of 400 and 600 ms at which  $I_{Kr}$  recruitment balances  $I_{Kur}$  block (35).  $I_{Kur}$  block rate-dependence, as described in this study, along with species- and remodeling-related differences, likely account for these conflicting results. Finally, genetic studies reported both loss- and gain-of-function variants associated with the development of lone AF (36–39). Whether and how these observations in rare genetically based forms of AF are applicable, remains to be seen more broadly.

$Na^+$  channel blockers (NCBs) are moderately effective antiarrhythmic drugs commonly used to control AF (40). In 2015, it was reported that  $I_{Kr}$  block increases the anti-AF effects of an optimized NCB by delaying repolarization at rapid rates (41). However,  $I_{Kr}$  blockers have reverse-use-dependent effects on APD, such that the APD-prolonging effect of  $I_{Kr}$  block is maximal at the slow rates of normal sinus rhythm (producing a serious risk of excess repolarization delay and ventricular proarrhythmia) and decreases markedly at rapid rates like those of AF. Given the positive rate-dependence of the APD-prolonging effect of  $I_{Kur}$  block, the addition of an  $I_{Kur}$  blocker to an optimized NCB would be expected to potentiate the NCB's anti-AF efficacy preferentially at rapid rates such as during AF. We have already shown evidence for this principle in a canine computational model (41). The work presented here provides tools and further rationale for testing this concept in human models.

### Study limitations

First, this study was performed *in silico* with extensive use of prior primary experimental patch-clamp data (2). The model predictions regarding the rate-dependent effects of  $I_{Kur}$  block on AP properties need to be tested prospectively in human tissue. Second, the model does not consider  $I_{Kur}$

modulation by adrenergic (42) or by vagal (30) tone, nor by temperature dependence (2). However, the model was based on data obtained at normal body temperature and should therefore be relevant to normal clinical conditions. Finally, as discussed above, we simulated  $I_{Kur}$  block with a fixed reduction in maximal conductance, whereas  $I_{Kur}$  block by antiarrhythmic drugs have been shown to depend on blocking kinetics and show state-dependent properties (22,29,43). Further computational analyses considering the state-dependent actions of specific  $I_{Kur}$  blockers might therefore be of interest.

Our simulations in remodeled atria have one major limitation. To compare remodeled results with those in non-remodeled conditions, we used the same  $I_{KACH}$  model and distributions. However,  $I_{KACH}$  is greatly reduced in remodeled atria (44). There are no realistic  $I_{KACH}$  models for remodeled atria. Future work is needed to create such models and use them to obtain a more accurate picture of  $I_{Kur}$ -blocking effects under these conditions.

## CONCLUSIONS

An updated *in silico* model that accounts for experimentally observed  $I_{Kur}$  inactivation kinetics shows that, contrary to possible intuitive inferences based on the potentially complete inactivation shown by  $I_{Kur}$ ,  $I_{Kur}$  inactivation is in fact negligible under physiologically relevant conditions. On the contrary, the main determinant of  $I_{Kur}$  rate dependence is the response of its activation dynamics to frequency-dependent changes in AP-morphology. However, despite a smaller absolute  $I_{Kur}$  magnitude at rapid rates, the relative contribution of  $I_{Kur}$  to AP repolarization increases because of decreases in offsetting currents, particularly  $I_{Kr}$ . These positive rate-dependent effects allow  $I_{Kur}$  block to terminate AF and position it to have potentially valuable antiarrhythmic properties. At the same time, our results also suggest that the efficacy of  $I_{Kur}$  block for AF termination might be greatly attenuated in the ionically remodeled atrium that develops after several days or more of sustained AF (8).

## SUPPORTING MATERIAL

Thirteen figures are available at [http://www.biophysj.org/biophysj/supplemental/S0006-3495\(17\)30341-7](http://www.biophysj.org/biophysj/supplemental/S0006-3495(17)30341-7).

## AUTHOR CONTRIBUTIONS

M.A. designed the study with the assistance of P.C. and S.N., performed all the simulations, analyzed the data and composed the manuscript. J.F. performed the original experimental work, provided all the original experimental data for analysis, and helped with the interpretation of the experimental results. E.V. provided the code for the AF simulation and assisted in its execution/analysis. P.C. supervised the modeling work and provided comments to improve the manuscript. S.N. supervised all aspects of the work, contributed to the original study concept and design, and helped with planning and completion of the manuscript.



## ACKNOWLEDGMENTS

We thank Jennifer Bacchi for expert secretarial assistance with the manuscript.

We acknowledge support through the Canadian Institutes of Health Research and Quebec Heart Foundation (S.N.), the Natural Sciences and Engineering Research Council (P.C.), and the Agence National de Recherche de France through the Investissements d'Avenir Program No. ANR-10-IAHU-04 (E.V.). Computations were made on the supercomputer Briare from Université de Montréal, managed by Calcul Québec and Compute Canada. The operation of this supercomputer is funded by the Canada Foundation for Innovation (CFI), the ministère de l'Économie, de la science et de l'innovation du Québec (MESI), and the Fonds de recherche du Québec - Nature et technologies (FRQ-NT).

## REFERENCES

- Wang, Z., B. Fermini, and S. Nattel. 1993. Sustained depolarization-induced outward current in human atrial myocytes. Evidence for a novel delayed rectifier K<sup>+</sup> current similar to Kv1.5 cloned channel currents. *Circ. Res.* 73:1061–1076.
- Feng, J., D. Xu, ..., S. Nattel. 1998. Ultrarapid delayed rectifier current inactivation in human atrial myocytes: properties and consequences. *Am. J. Physiol.* 275:H1717–H1725.
- Ford, J., J. Milnes, ..., U. Ravens. 2016. The positive frequency-dependent electrophysiological effects of the I<sub>Kur</sub> inhibitor XEN-D0103 are desirable for the treatment of atrial fibrillation. *Heart Rhythm.* 13:555–564.
- Courtemanche, M., R. J. Ramirez, and S. Nattel. 1998. Ionic mechanisms underlying human atrial action potential properties: insights from a mathematical model. *Am. J. Physiol.* 275:H301–H321.
- Kneller, J., R. Zou, ..., S. Nattel. 2002. Cholinergic atrial fibrillation in a computer model of a two-dimensional sheet of canine atrial cells with realistic ionic properties. *Circ. Res.* 90:E73–E87.
- Vigmond, E. J., M. Hughes, ..., L. J. Leon. 2003. Computational tools for modeling electrical activity in cardiac tissue. *J. Electrocardiol.* 36:69–74.
- Pandit, S. V., O. Berenfeld, ..., J. Jalife. 2005. Ionic determinants of functional reentry in a 2-D model of human atrial cells during simulated chronic atrial fibrillation. *Biophys. J.* 88:3806–3821.
- Courtemanche, M., R. J. Ramirez, and S. Nattel. 1999. Ionic targets for drug therapy and atrial fibrillation-induced electrical remodeling: insights from a mathematical model. *Cardiovasc. Res.* 42:477–489.
- Feng, J., B. Wible, ..., S. Nattel. 1997. Antisense oligodeoxynucleotides directed against Kv1.5 mRNA specifically inhibit ultrarapid delayed rectifier K<sup>+</sup> current in cultured adult human atrial myocytes. *Circ. Res.* 80:572–579.
- Philipson, L. H., R. E. Hice, ..., D. F. Steiner. 1991. Sequence and functional expression in *Xenopus* oocytes of a human insulinoma and islet potassium channel. *Proc. Natl. Acad. Sci. USA.* 88:53–57.
- Snyders, D. J., M. M. Tamkun, and P. B. Bennett. 1993. A rapidly activating and slowly inactivating potassium channel cloned from human heart. Functional analysis after stable mammalian cell culture expression. *J. Gen. Physiol.* 101:513–543.
- Firek, L., and W. R. Giles. 1995. Outward currents underlying repolarization in human atrial myocytes. *Cardiovasc. Res.* 30:31–38.
- Amos, G. J., E. Wettwer, ..., U. Ravens. 1996. Differences between outward currents of human atrial and subepicardial ventricular myocytes. *J. Physiol.* 491:31–50.
- Koidl, B., P. Flaschberger, ..., B. Rigler. 1996. Effects of the class III antiarrhythmic drug ambasilide on outward currents in human atrial myocytes. *Naunyn-Schmiedeberg's Arch. Pharmacol.* 353:226–232.
- Zaza, A. 2010. Control of the cardiac action potential: the role of repolarization dynamics. *J. Mol. Cell. Cardiol.* 48:106–111.
- Bányász, T., B. Horváth, ..., P. P. Nánási. 2009. Reverse rate dependency is an intrinsic property of canine cardiac preparations. *Cardiovasc. Res.* 84:237–244.
- Cummins, M. A., P. J. Dalal, ..., E. A. Sobie. 2014. Comprehensive analyses of ventricular myocyte models identify targets exhibiting favorable rate dependence. *PLoS Comput. Biol.* 10:e1003543.
- Knobloch, K., J. Brendel, ..., K. J. Wirth. 2002. Electrophysiological and antiarrhythmic effects of the novel I<sub>Kur</sub> channel blockers, S9947 and S20951, on left vs. right pig atrium in vivo in comparison with the I<sub>Kr</sub> blockers dofetilide, azimilide, d,l-sotalol and ibutilide. *Naunyn-Schmiedeberg's Arch. Pharmacol.* 366:482–487.
- Blaauw, Y., H. Gögelein, ..., M. A. Allesie. 2004. "Early" class III drugs for the treatment of atrial fibrillation: efficacy and atrial selectivity of AVE0118 in remodeled atria of the goat. *Circulation.* 110:1717–1724.
- Fedida, D., P. M. R. Orth, ..., G. N. Beatch. 2005. The mechanism of atrial antiarrhythmic action of RSD1235. *J. Cardiovasc. Electrophysiol.* 16:1227–1238.
- Dorian, P., A. Pinter, ..., G. N. Beatch. 2007. The effect of vernakalant (RSD1235), an investigational antiarrhythmic agent, on atrial electrophysiology in humans. *J. Cardiovasc. Pharmacol.* 50:35–40.
- Scholz, E. P., P. Carrillo-Bustamante, ..., G. Seemann. 2013. Rotor termination is critically dependent on kinetic properties of I<sub>Kur</sub> inhibitors in an in silico model of chronic atrial fibrillation. *PLoS One.* 8:e83179.
- Roy, D., C. M. Pratt, ..., A. J. Camm; Atrial Arrhythmia Conversion Trial Investigators. 2008. Vernakalant hydrochloride for rapid conversion of atrial fibrillation: a phase 3, randomized, placebo-controlled trial. *Circulation.* 117:1518–1525.
- van Hunnik, A., D. H. Lau, ..., U. Schotten. 2016. Antiarrhythmic effect of vernakalant in electrically remodeled goat atria is caused by slowing of conduction and prolongation of postrepolarization refractoriness. *Heart Rhythm.* 13:964–972.
- Lagrutta, A., J. Wang, ..., J. J. Salata. 2006. Novel, potent inhibitors of human Kv1.5 K<sup>+</sup> channels and ultrarapidly activating delayed rectifier potassium current. *J. Pharmacol. Exp. Ther.* 317:1054–1063.
- Valenzuela, C., E. Delpón, ..., D. J. Snyders. 1996. Class III antiarrhythmic effects of zatebradine. Time-, state-, use-, and voltage-dependent block of hKv1.5 channels. *Circulation.* 94:562–570.
- Delpón, E., C. Valenzuela, ..., J. Tamargo. 1997. Block of human cardiac Kv1.5 channels by loratadine: voltage-, time- and use-dependent block at concentrations above therapeutic levels. *Cardiovasc. Res.* 35:341–350.
- Choi, B. H., J.-S. Choi, ..., M.-S. Kim. 2000. Direct block by bisindolylmaleimide of rat Kv1.5 expressed in Chinese hamster ovary cells. *J. Pharmacol. Exp. Ther.* 293:634–640.
- Tsujiima, K., S. Suzuki, ..., Y. Kurachi. 2007. Frequency-dependent effects of various I<sub>Kr</sub> blockers on cardiac action potential duration in a human atrial model. *Am. J. Physiol. Heart Circ. Physiol.* 293:H660–H669.
- Rivard, L., A. Shiroshita-Takeshita, ..., S. Nattel. 2005. Electrophysiological and atrial antiarrhythmic effects of a novel I<sub>Kur</sub>/Kv1.5 blocker in dogs. *Heart Rhythm.* 2:S180.
- Shiroshita-Takeshita, A., C. Maltais, ..., S. Nattel. 2006. Electrophysiological and atrial antiarrhythmic effects of a novel I<sub>Kur</sub>/Kv1.5 blocker in dogs with atrial tachycardia remodeling. *Heart Rhythm.* 3:S183.
- Ford, J., J. Milnes, ..., U. Ravens. 2013. Human electrophysiological and pharmacological properties of XEN-D0101: a novel atrial-selective Kv1.5/I<sub>Kur</sub> inhibitor. *J. Cardiovasc. Pharmacol.* 61:408–415.
- Burashnikov, A., and C. Antzelevitch. 2008. Can inhibition of I<sub>Kur</sub> promote atrial fibrillation? *Heart Rhythm.* 5:1304–1309.
- Yue, L., Z. Wang, ..., S. Nattel. 2000. Molecular evidence for a role of Shaw (Kv3) potassium channel subunits in potassium currents of dog atrium. *J. Physiol.* 527:467–478.

35. Pavri, B. B., H. E. Greenberg, ..., D. Bloomfield. 2012. MK-0448, a specific Kv1.5 inhibitor: safety, pharmacokinetics, and pharmacodynamic electrophysiology in experimental animal models and humans. *Circ. Arrhythm. Electrophysiol.* 5:1193–1201.
36. Olson, T. M., A. E. Alekseev, ..., A. Terzic. 2006. Kv1.5 channelopathy due to KCNA5 loss-of-function mutation causes human atrial fibrillation. *Hum. Mol. Genet.* 15:2185–2191.
37. Yang, T., P. Yang, ..., D. Darbar. 2010. Novel KCNA5 mutation implicates tyrosine kinase signaling in human atrial fibrillation. *Heart Rhythm.* 7:1246–1252.
38. Christophersen, I. E., M. S. Olesen, ..., N. Schmitt. 2013. Genetic variation in KCNA5: impact on the atrial-specific potassium current  $I_{Kur}$  in patients with lone atrial fibrillation. *Eur. Heart J.* 34:1517–1525.
39. Hayashi, K., T. Konno, ..., M. Yamagishi. 2015. Functional characterization of rare variants implicated in susceptibility to lone atrial fibrillation. *Circ. Arrhythm. Electrophysiol.* 8:1095–1104.
40. Aguilar, M., and S. Nattel. 2015. The past, present, and potential future of sodium channel block as an atrial fibrillation suppressing strategy. *J. Cardiovasc. Pharmacol.* 66:432–440.
41. Aguilar, M., F. Xiong, ..., S. Nattel. 2015. Potassium channel blockade enhances atrial fibrillation-selective antiarrhythmic effects of optimized state-dependent sodium channel blockade. *Circulation.* 132:2203–2211.
42. Li, G. R., J. Feng, ..., S. Nattel. 1996. Adrenergic modulation of ultra-rapid delayed rectifier  $K^+$  current in human atrial myocytes. *Circ. Res.* 78:903–915.
43. Almquist, J., M. Wallman, ..., M. Jirstrand. 2010. Modeling the effect of Kv1.5 block on the canine action potential. *Biophys. J.* 99:2726–2736.
44. Dobrev, D., E. Graf, ..., U. Ravens. 2001. Molecular basis of downregulation of G-protein-coupled inward rectifying  $K^+$  current ( $I_{K,Ach}$ ) in chronic human atrial fibrillation: decrease in GIRK4 mRNA correlates with reduced ( $I_{K,Ach}$ ) and muscarinic receptor-mediated shortening of action potentials. *Circulation.* 104:2551–2557.